



# The phase change property of lauric acid confined in carbon nanotubes as nano-encapsulated phase change materials

Shuying Wu<sup>1</sup> · Xinyao Ma<sup>1</sup> · Deqi Peng<sup>1</sup> · Yebin Bi<sup>1</sup>

Received: 1 February 2018 / Accepted: 4 November 2018 / Published online: 14 November 2018  
© Akadémiai Kiadó, Budapest, Hungary 2018

## Abstract

Lauric acid (LA) impregnates in carbon nanotubes (CNTs), resulting in nano-encapsulated phase change materials (PCMs). TEM and DSC results both indicate that the filling of LA into CNTs is realized by the vacuum infiltration method. A further study of nano-encapsulated PCMs at the molecular level is investigated by molecular dynamics simulations. From the axial view of CNTs, LA molecules always keep a circular distribution inside CNTs with a radius of about 4.8 Å. The analysis on radial distribution function, the end-to-end distance and the torsion angle simultaneously verifies that the order degree of LA molecules is improved due to the nano-confined effect of CNTs. The diffusion coefficient of LA is enhanced in CNTs. The energy flux and thermal conductivity of LA molecules in CNTs are higher than those of pure LA at the same temperature. These results fully indicate the heat and mass transfer of LA in CNTs could be enhanced. The current research could contribute to a deep understanding nanoscale thermal science and to potential application in heat dissipation of nanodevices.

**Keywords** Lauric acid · Carbon nanotubes · Nano-confined effect · Phase change material · Molecular dynamics simulation

## Introduction

Due to the intensified energy crisis and the increasing environmental issues, energy storage technology using phase change materials (PCMs) has received much attention [1–3]. Fatty acids, such as lauric acid (LA), have the advantages of low cost, high latent heat, low supercooling degree, wide availability and excellent thermal stability [4, 5]. Moreover, their major disadvantage is the low heat transfer rate. Many methods are proposed to solve this problem, such as dispersing various carbon materials [6, 7] or porous materials into PCMs [1, 8] and preparing encapsulated materials [9, 10].

CNTs, well known for having high thermal conductivity (2000–6000 W m<sup>-1</sup> K<sup>-1</sup>) [11], are mainly used as an effective nano-filler for enhancing thermal conductivity [12–14]. However, there is limited research on using the hollow cavity of CNTs to study heat transfer. The massive

studies have proved substances exhibit the unique behaviors under the confinement condition [15–17]. Calorimetric studies evidenced that poly(ethylene glycol), encapsulated in polystyrene fibers, showed a non-trivial crystallization behavior [17]. Recently, a new kind of nano-encapsulated PCMs is proposed to solve the low thermal conductivity trouble and avoid the solidification on the heat transfer surface by filling PCMs into CNTs [18, 19]. The van der Waals interactions between confined molecules and the confining wall prevent molecules to escape from the hollow CNTs [20–22]. The intercalation of paraffin into CNTs as a liquid coolant has been verified to enhance the heat transfer rate and decrease the temperature of microelectronic devices, which was due to the latent heat of paraffin [18]. The study on the nanoscale heat transfer of sugar alcohols filling in CNTs pointed out that the heat transfer rate was dependent on the material, the CNT diameter and structure [23]. In the intercalation experiment, paraffin outside of CNTs could be completely removed by appropriate solvent treatment, while that inside CNTs won't be washed away [24]. Different types of paraffins and their mixtures could be filled into CNTs as nano-encapsulated PCMs with a smart tunable working temperature [19]. The

✉ Shuying Wu  
wusy2015@xtu.edu.cn

<sup>1</sup> School of Mechanical Engineering, Xiangtan University, Xiangtan 411105, Hunan, People's Republic of China

favorable free energy inside CNTs was the driving force in these systems [25]. However, it is limited and difficult to investigate the deeper mechanism only by experimental methods. MD method is suitable to analyze the microcosmic or mesoscopic structure dynamic change and characteristic [26, 27]. The torsion and extension of *n*-octadecane molecule chains were restricted by excessive thick shell in the nano-encapsulated PCM system [28]. The introduction of CNTs and graphene layers into paraffin led to liquid molecule ordering and thermal conductivity enhancement [29]. In our previous study, it has proved that nano-confined environment of CNTs played an important role in the structure and thermal property of paraffin [30, 31]. The thermal conductivity of *n*-heptacosane was enhanced when it was confined in CNTs [31]. The reported papers show that this kind of nano-encapsulated PCM has a great potential in heat dissipation. Future progress and technological advances for utilizing confined PCMs in various nanostructures would undoubtedly depend on obtaining a basic understanding of the phase change property in these systems.

In this paper, the filling of LA into CNTs as a nano-encapsulated PCM was performed with a vacuum infiltration method. TEM and DSC measurements proved the successful filling. To further understand nano-confined effect on the structure and phase change property of LA, molecule distribution, RDF, end-to-end distance, torsion angle, self-diffusion coefficient and thermal conductivity were analyzed by MD simulation.

## Experimental

### Experimental methods

#### Filling

Firstly, the pristine CNTs (Chengdu Organic Chemicals Co., Ltd., China; inner diameter: 30–50 nm, outer diameter: 50–60 nm, length: 5–30  $\mu\text{m}$ , specific area:  $120 \text{ m}^2 \text{ g}^{-1}$ ) were treated with concentrated nitric acid to open the closed ends and purify using the same method in our previous paper [30]. LA (Sinopharm Group Chemical Reagent Co., Ltd., China) was dispersed in anhydrous ethanol with a mass ratio of 1: 4 and sonicated for 15 min to obtain a stable homogeneous solution. Then, the opened end CNTs were put into a sealed flask in an oil bath with 80  $^{\circ}\text{C}$ . A vacuum pump was used to drive away the air in the flask and CNTs. Next, the solution was quickly injected into the flask and retained for 20 min. To well disperse CNTs in the solution, the magnetic stirring treatment was implemented during the filling process. Afterward, the mixture was filtered with anhydrous ethanol to remove the

LA residuals outside the CNTs. Finally, the obtained product was dried at normal temperature and pressure.

### Characterization

The microphotography of the materials was examined with transmission electron microscopy (TEM) (JEM-2100F). The phase change properties were analyzed by DSC (DSC-Q10, TA Instrument Inc., USA) with a scanning rate at  $5 \text{ }^{\circ}\text{C min}^{-1}$ .

### Simulation methods

To understand the nano-confined effect of CNT on LA, two MD models were constructed as shown in Fig. 1: (a) LA freestanding system containing 15 molecules in a  $16.5 \times 16.5 \times 16.5 \text{ \AA}$  box; (b) LA confined in CNT in a  $37.2 \times 37.2 \times 61.5 \text{ \AA}$  box. The number of LA molecules was effectively based on the experimental results. Considering the computation load and our concern, which was the interaction of LA and the inner wall of CNT, a single-wall (25, 25) CNT model was constructed with 2500 carbon atoms.

After the initial structure was built, the smart minimization method was performed to optimize the geometry. To refine the conformation, six anneal cycles were exerted from 288 to 348 K at a speed of  $1 \text{ K ps}^{-1}$  under micro canonical (NVE) ensemble. The energy curve during the annealing process is shown in Fig. 2. Fluctuation of energy curve means the storage and release of heat energy [28]. In this process, the system continuously adjusted the structure to make itself cross the energy barrier. After the anneal operation, the systems were pre-equilibrated with 200 ps and run 800 ps for the data collection under isothermal isobaric (NPT) ensemble at each temperature rising simulation with an interval of 10 K from 288 to 348 K. As shown in Fig. 3, the density of LA fluctuates at  $0.89 \text{ g cm}^{-3}$  in agreement with the experiment value [32], validating the choice of the simulated method. Meanwhile,

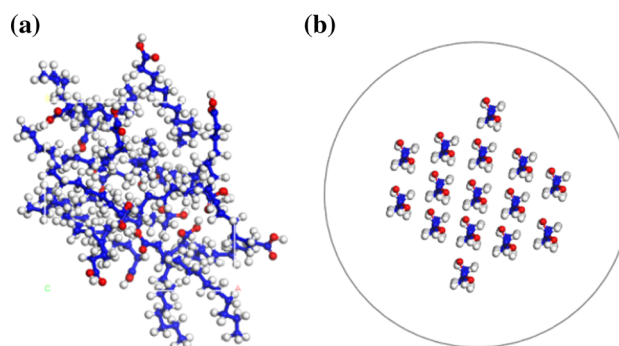


**Fig. 1** Initial structures of **a** LA freestanding system **b** LA confined in CNT

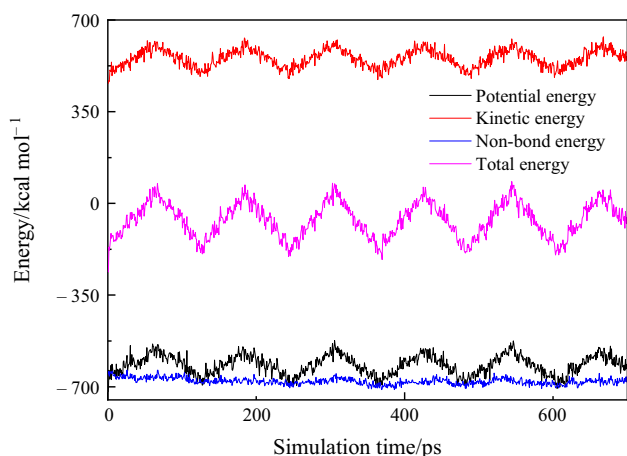


**Fig. 2** Energy fluctuating curve of LA during the anneal process

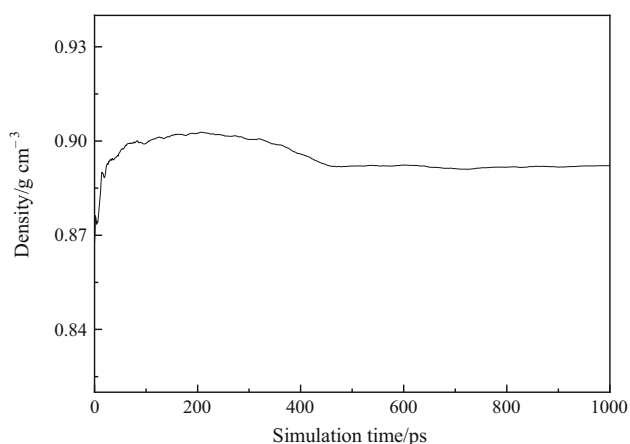


**Fig. 3** Density curve of LA during the dynamics process

the density value remains unchanged in 450–1000 ps, which indicates that the simulated time of 1000 ps is sufficient for the current system. In the simulation process, the condensed-phase optimized molecular potentials for atomistic simulation study (COMPASS) force field could preferably describe the organic systems. The time step was set as 1 fs, and the periodic boundary conditions were fixed in  $x$ ,  $y$  and  $z$  directions. Andersen's thermostat and Berendsen's barostat methods were used to control the temperature and pressure, respectively.

Reverse non-equilibrium molecular dynamics (RNEMD) method was introduced to calculate the thermal conductivity of each system at 298 K [33]. The method is based on the Fourier heat conduction law:

$$\lambda = \lim_{dT/dz \rightarrow 0} \lim_{t \rightarrow 0} \frac{J_z(t)}{dT/dz} \quad (1)$$

where  $dT/dz$  denotes the temperature gradient in  $z$  direction and  $J_z(t)$  is the heat flux.

In RNEMD method, each system is evenly divided into 40 layers in  $z$  direction. The middle layer is set as the cool slab, while both ends are set as the hot slab. The particles, whose kinetic energy is the largest in the cold region, are selected to exchange energy and momentum with the particles whose kinetic energy is the lowest in the hot region. Through this operating, the temperature gradient between the cool and the hot slab is produced. After the systems reach to steady state, the unphysical energy exchange is balanced by the physical thermal conduction in the systems and the stable temperature gradient is established. Thus, the imposed heat flux could be calculated by summing up the energy exchanges in the two slabs through the following expression

$$\langle J_z(t) \rangle = \frac{1}{2At} \sum_{\text{transfer}(t)} \frac{1}{2} m_h \left( (v_h^{\text{new}})^2 - (v_h^{\text{old}})^2 \right) \quad (2)$$

where  $A$  is the cross-sectional area,  $m_h$  is the respective mass of the particles selected for energy exchange in hot slabs, and  $(v_h^{\text{new}})$  and  $(v_h^{\text{old}})$  present the new and old velocity of the selected particles in the cold region.

Besides, the kinetic temperature  $T_k$  in slab  $k$  could be determined by

$$T_k = \frac{1}{3n_k k_B} \sum_{i \in h}^{n_k} m_i v_i^2 \quad (3)$$

where the sum extends over the  $n_k$  particles  $i$  in slab  $k$  with mass  $m_i$  and velocity  $v_i$ ,  $k_B$  is Boltzmann's constant. As a result, the stable temperature gradient could be easily achieved.

The RNEMD calculations for each system were carried out on the base of the corresponding balanced structures. Before sampling process, both systems were further balanced. Considering the complexity of confined system, the simulation time of balanced stage for pure LA system and confined system was 100 ps and 200 ps, respectively. And the sampling process for thermal conductivity for both systems was 500 ps and 1000 ps, respectively.

## Results and discussion

### Analysis of TEM

Figure 4 shows the TEM image of CNTs filled with LA. As can be seen, the residual impurity in CNTs powder generated in the production process was removed under the action of concentrated nitric acid. The ends of CNTs are opened, which provide the possibility of the successful filling. Some CNTs keep empty shown with the black arrow, while some CNTs are filled with LA, shown with the red arrow and the red ring. There is a gap at the

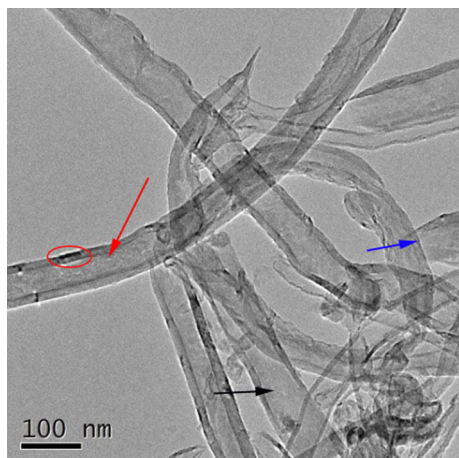


**Fig. 4** TEM image of CNTs filled with LA. The blue arrow indicates the opened end. The black arrow indicates the empty cavity. The red arrow indicates LA filled in CNTs. The red ring indicates the gap. (Color figure online)

interface between CNTs and LA. It is difficult for LA escaping from CNTs due to the irregular configuration of LA in nanochannel [34].

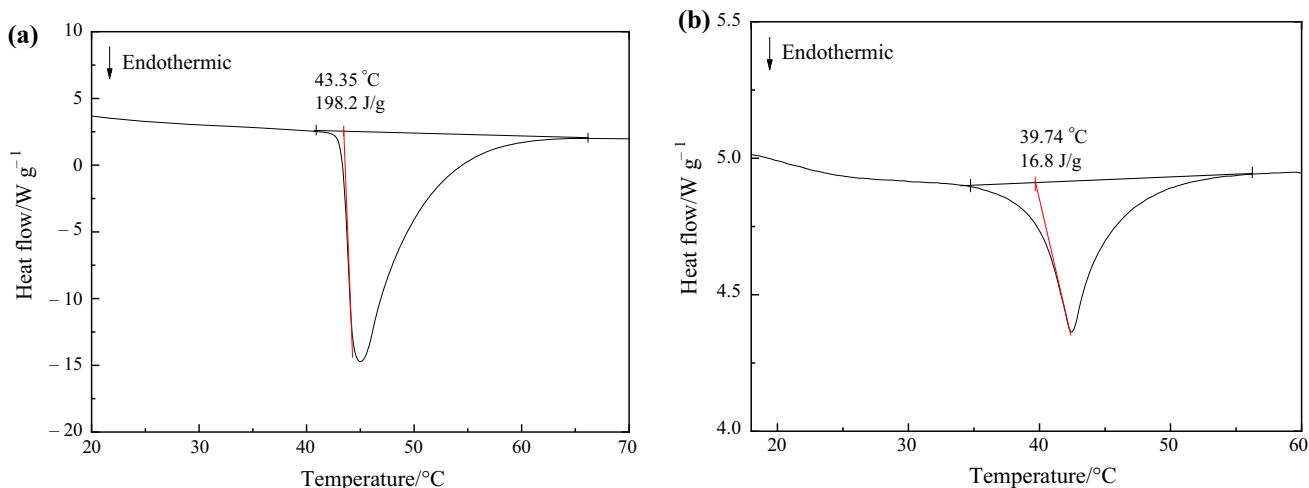
### Thermal property of LA confined in CNT

Figure 5 shows DSC curves of LA in freestanding and confined systems. For both systems, there are endothermic peaks in the range of 20–70 °C. Due to the absence of phase change of CNTs, the endothermic peak in the confined system could attribute to LA. It undoubtedly verifies that LA is successfully infiltrated into CNTs. The melting temperatures of LA in freestanding and confined state are 43.35 °C and 39.74 °C, respectively. The decrease in the melting temperature is caused by the confinement effect of CNTs [17, 24]. Gradys A. stated that the crystallization of

PCMs in confinement environment changed from heterogeneous nucleation with three-dimensional crystal growth to two- and one-dimensional, terminated by homogenous nucleation [17]. The structural changes of LA will be found in the following MD discussion. The latent heats are  $198.2 \text{ J g}^{-1}$  and  $16.78 \text{ J g}^{-1}$  for two systems, respectively, which means that the mass percentage of LA confined in CNT is 8.5%. Compared with the mass fraction, the degree of filling, which is denoted as the volume of PCM versus the volume of empty CNTs, could better reflect the availability of empty CNTs. The degree of filling of LA inside CNTs is 10.02% according to the calculated method mentioned in our previous paper [30]. It indicates that the complete filling is not obtained and the degree of filling could be further improved. Furthermore, it could conclude that there is 15 LA molecules confined in CNTs, which will be used to determine the initial structure in the next MD simulations.

### The structure of LA confined in CNT

The thermo-physical property of materials is closely related to their structures. The final structures of LA in freestanding and confined systems are obtained by running 1000 ps dynamic simulations at 298 K and 348 K, respectively, which represent solid and liquid states. As shown in Fig. 6, the molecule distribution of LA in the freestanding state has a remarkable distinguish from that confined in CNT. Due to the inductive effect of CNT, LA molecules become an orderly arrangement in nano-confined environment, which is different from the chaotic structure of LA molecules in freestanding systems. Aoun et al. [20] also stated that it was a well-ordered organization of water molecules under CNT confinement. A highly orderly structure has a potentially positive effect



**Fig. 5** DSC curves of **a** LA and **b** LA confined in CNTs

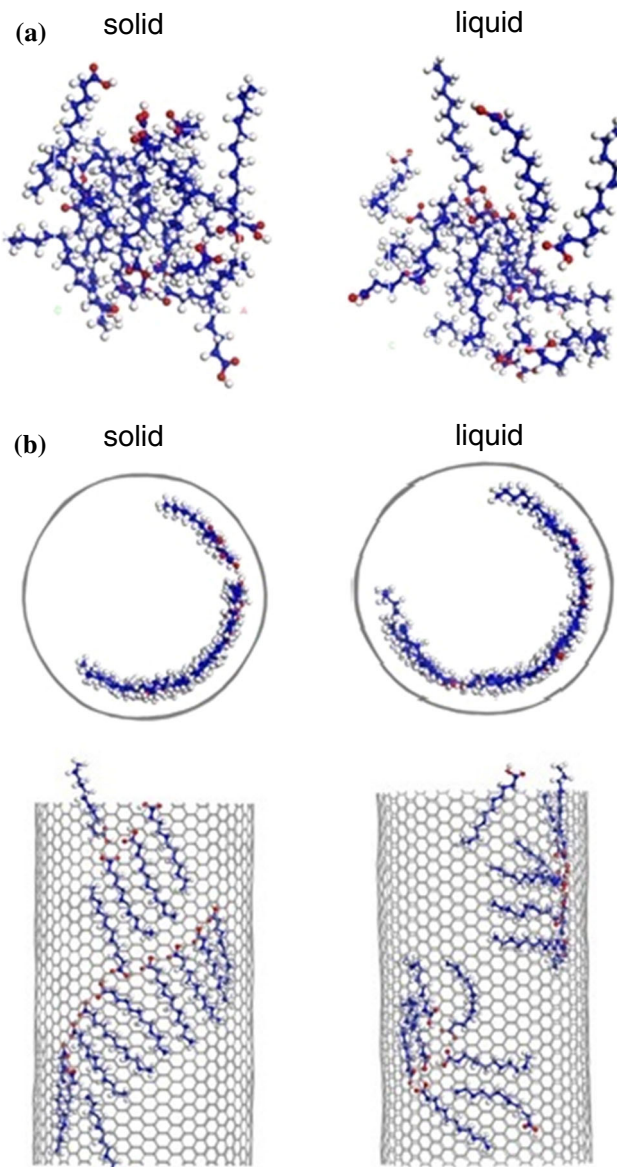


**Fig. 6** Structures of LA in freestanding (a) and confined (b) systems

on thermal conductivity [35]. From the axial view of CNT, LA molecules are always in a circular distribution inside CNT with a radius of about 13.15 Å. The radius of CNT is 16.95 Å. Thus, the distance between LA molecules and tube wall of CNT is 4.8 Å, which is in the range of the van der Waals force [21]. Probably due to this interaction force, LA molecules orderly distribute in CNT and do not easily outflow from the inner space of CNT during the phase change process, which has been verified by the simulation and experimental methods [20, 22]. Liang et al. [22] reported there was no leakage of PCMs from halloysite clay nanotubes even after 200 heating and cooling cycles. Meanwhile, the molecule distribution in the freestanding and confined systems at liquid state is more disordered than that at solid state due to the thermal motion.

## RDF, end-to-end distance and torsion angle

The above-obtained structures provide intuitive and simple illustrations of the order of LA molecules. However, this method is subjective and easily affected by the observer's visual angle. Fortunately, the analysis of RDF, end-to-end distance and torsion angle provides an accurate and objective way to study the order of current systems.

RDF  $g(r)$  could be considered to reflect the molecule structure. It represents the atomic density varying as a function of the distance  $r$  from one particular atom, which could be expressed as the following equation [36]:

$$g(r) = \frac{1}{\rho 4\pi r^2} \cdot \frac{\sum_{t=1}^K \sum_{j=1}^N \Delta N(r \rightarrow r + \delta r)}{N \cdot K} \quad (4)$$

where  $\rho$  is the overall number density,  $N$  is the total number of atoms,  $K$  is the number of time steps, and  $\delta r$  is the distance interval.

The RDF with temperature is shown in Fig. 7. Compared with LA in freestanding state, the position of the first peak of LA in CNT shifts from 2.0 to 1.5 Å. The reason is that the inner wall of CNT restricts the motion of LA molecules, which will result in the perfect molecule structure [37]. Due to the good inter-molecular attraction between LA and CNTs, the peak intensities of LA in CNT is obviously enhanced, which certifies the enhancement of the thermal response. In other words, the addition of CNT will enhance the heat conduction [26, 31]. According to the partial enlarged view, the RDF peaks of LA in freestanding and confined systems become weaker along with the increase in temperature. The reason is that the mobility of LA molecules increases and the order parameter decreases. Simultaneously, there is an abrupt decrease in the first peak at 318–328 K and 308–318 K for the freestanding and confined system, respectively. It is corresponded to the phase change process, which is in a good agreement with the above experimental results.

In order to further understand the extension of LA molecule chains, the end-to-end distance and the torsion angle are discussed in Figs. 8 and 9. The end-to-end distance is the distance of the two carbon atoms at both ends of LA molecule chains, which is an average value. The torsion angle is set among the four neighboring C atoms [28].

As shown in Fig. 8, the peaks of end-to-end distance of LA molecules in CNT are high and narrow, but in the freestanding system, low and wide. The end-to-end distances mainly distribute in the range of 7–15.5 and 10–15.5 Å for LA molecules in the freestanding and confined states, respectively. And the main peaks are observed at about 12 Å for the freestanding state, 14 and 15 Å for the confined state. It suggests that LA molecule chain gets

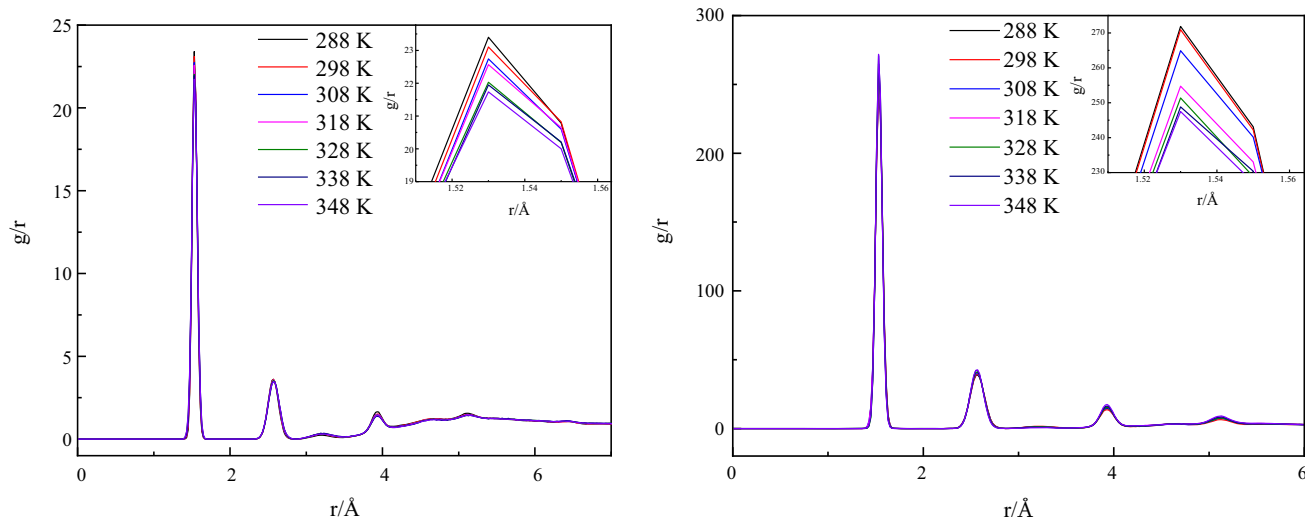


**Fig. 7** RDF of LA in freestanding (a) and confined (b) systems with temperature

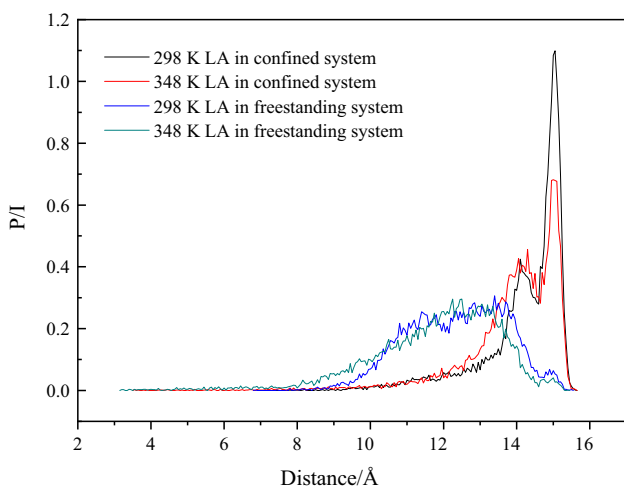


**Fig. 8** End-to-end distance distribution of LA molecules in free-standing and confined systems

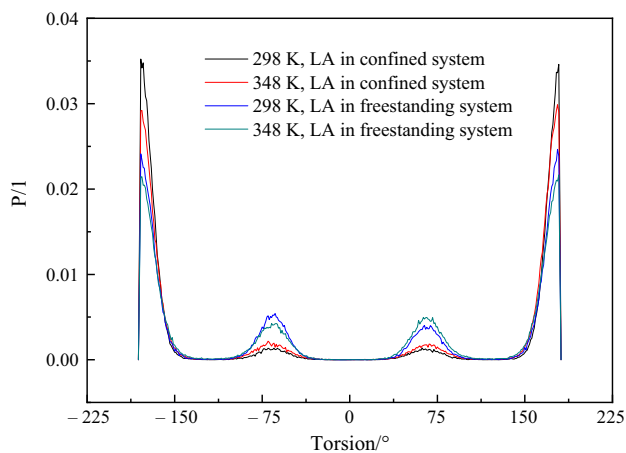


**Fig. 9** Torsion angle distribution of LA molecules in free-standing and confined systems

the better extension due to the constrained action of CNT compared with that in freestanding state. Therefore, the mass transfer of system will be enhanced [26]. Moreover, the distribution range of the end-to-end distance at 348 K is slightly increased compared with that at 298 K, which verifies the increase in the molecule diffuse along with the increasing temperature.

Figure 9 shows the torsion angle distribution of LA molecules in freestanding and confined systems at 298 K and 348 K, which has a consistent trend. The main peaks are both observed at about  $\pm 180^\circ$  and  $\pm 65^\circ$ , respectively. However, the peak variation is obvious due to the confined effect of CNT. Comparing with the freestanding system, the distribution increases at  $\pm 180^\circ$  and decreases at  $\pm 65^\circ$  in the confined system. It could be concluded that CNT restricts the torsion of LA molecules and makes LA molecules have a good extension, which is in agreement with the analysis of the end-to-end distance. For both systems, the peak height decreases at  $\pm 180^\circ$  and increases at  $\pm 65^\circ$  from 298 to 348 K. This indicates that the torsion degree and thermal motion of LA molecules strengthen. The investigation of the end-to-end distance and torsion angle simultaneously suggests that the torsion and tensile behavior of LA molecular chains are closely related to the confinement action of CNT.

### Diffusion coefficient

In order to investigate the dynamics of LA molecules in the nano-confined environment, the diffusion coefficient  $D$  was calculated according to the well-known Einstein equation [22]:

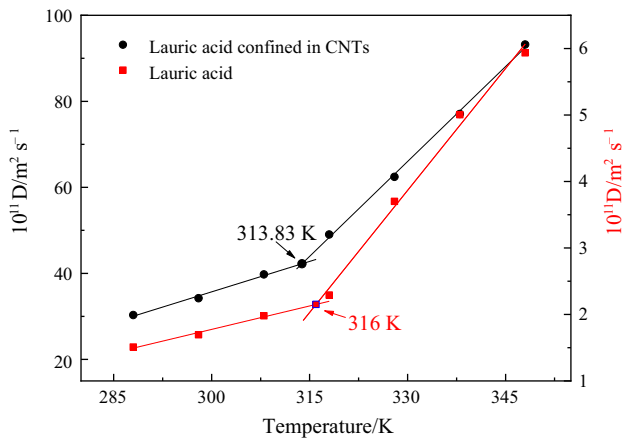


Fig. 10 Self-diffusion coefficient as a function of temperature

$$D = \frac{1}{6N} \lim_{t \rightarrow \infty} \frac{d}{dt} \sum_{i=1}^N \langle |r_i(t) - r_i(0)|^2 \rangle \quad (5)$$

where  $N$  is the number of atoms,  $t$  is the simulation time,  $r_i(t)$  is the position vector of  $i$ th particle at time  $t$ ,  $r_i(0)$  is the position vector of  $i$ th particle at the origin time, and the angular brackets are the ensemble average.

From Fig. 10, the diffusion coefficient of two systems increases with temperature. The high temperature sections diffuse more intensely than the low-temperature sections due to the molecular thermal motion. The curves trends are consistent, which proves that LA molecules have similar diffusion behavior under the influence of CNT. In addition, the effect of the nano-confined environment enhances the diffusion intensity of the LA molecules. For example, at 328 K, the diffusion coefficients of LA molecules in CNT and in the freestanding system are  $6.24 \times 10^{-10} \text{ m}^2 \text{ s}^{-1}$

and  $3.7 \times 10^{-11} \text{ m}^2 \text{ s}^{-1}$ , respectively. The enhancement of diffusion coefficient means the increase in thermal conductivity [38], which is favorable for a new kind of PCMs.

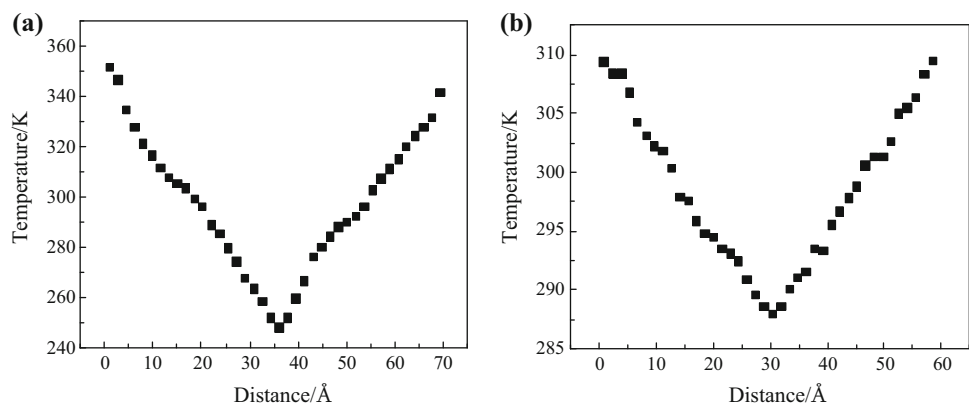
As presented by Rao et al. [26], the values of diffusion coefficient could be fitted into two straight lines. And the intersection point of the two lines is regarded as the melting temperature of  $n$ -alkane. So, the melting temperatures of LA in freestanding and confined systems are 315.98 and 313.83 K, which has a good agreement with experimental data with 0.84% and 2% error, respectively. It indicates that the MD simulation method is reasonable for current systems.

### Thermal conductivity

It is complicated, inaccurate and time consuming to measure the thermal conductivity of the low-dimensional systems by the experimental method. However, MD method is convenient to predict this parameter. Figure 11 presents the temperature gradient of LA in freestanding and confined systems. The average temperatures decrease linearly from the hot slab to the cold slab, which indicates that the stable temperature gradient is established.

Figure 12 shows the energy flux and thermal conductivity curves of LA in freestanding and confined systems at 298 K. The values are convergent at 250 ps and 750 ps for LA in freestanding and confined systems, respectively, which is due to the complexity of the latter. It suggests that the current simulated time is enough to evaluate the thermal conductivity. The convergent values of energy flux for freestanding and confined systems are 4.93 and 29.67  $\text{GW m}^{-2}$ , respectively, and 69.50  $\text{GW m}^{-2}$  for empty CNT. The highly order of LA molecules in the nano-confined environment enhances the energy and heat transfer

Fig. 11 Temperature gradient of LA in freestanding (a) and confined (b) systems



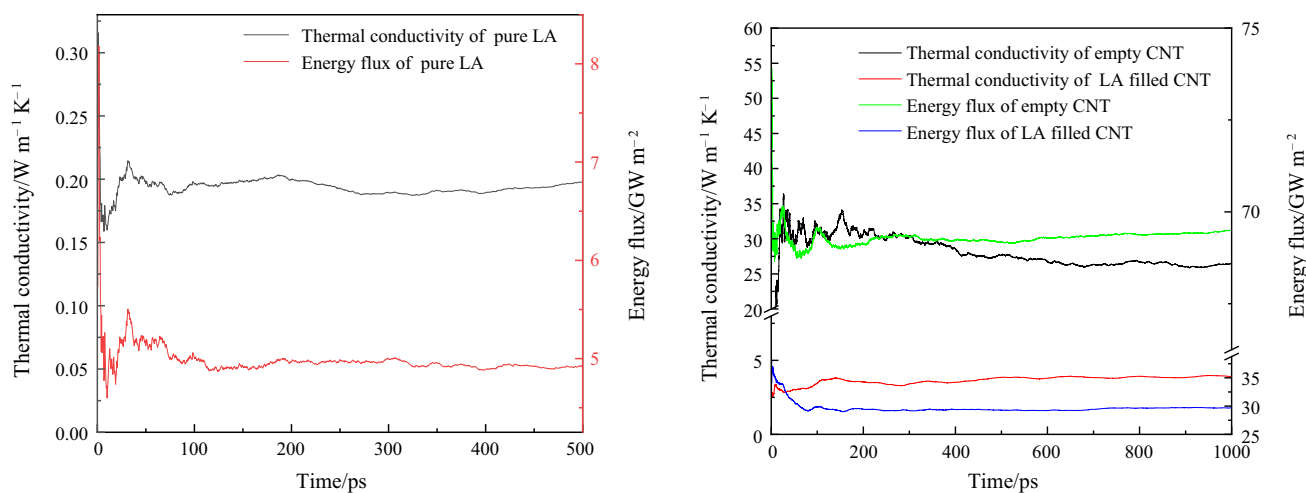


**Fig. 12** Energy flux and thermal conductivity curves of LA in freestanding (a) and confined (b) systems at 298 K

rate. Finally, it will result in the enhancement of thermal conductivity. Meanwhile, the constructive phonons coupling between LA molecules and CNT is favorable for enhancing the thermal conductivity. The thermal conductivity of pure LA is  $0.2 \text{ W m}^{-1} \text{ K}^{-1}$  closely with the experimental value  $0.215 \text{ W m}^{-1} \text{ K}^{-1}$  [39]. Thermal conductivity of CNT is  $26.43 \text{ W m}^{-1} \text{ K}^{-1}$ , which is in good agreement with the reported values [40]. The thermal conductivity of LA filled in CNTs is  $3.91 \text{ W m}^{-1} \text{ K}^{-1}$  which is about 20 times of bulk LA. The enhancement of thermal conductivity for LA is much higher than that of composite PCMs prepared by traditional methods [41]. The similar result has also been reported by many authors [42, 43]. Yutaka et al. [42] claimed that the calculated effective thermal conductivity of the ionic liquid filled into CNTs increases to  $19.9 \text{ W m}^{-1} \text{ K}^{-1}$ , which is much larger than the pure material with  $0.2 \text{ W m}^{-1} \text{ K}^{-1}$ .

## Conclusions

The phase change property of LA confined in CNTs as nano-encapsulated PCMs is systemically studied by the combination of experiment and MD simulation. With the vacuum infiltration method, the successful filling of LA into CNTs is proven by TEM and DSC. The melting temperature of LA decreases from 316.5 to 312.89 K, which is also verified by MD simulation. The degree of filling of LA in CNTs is 10.02%. MD simulations suggest that LA molecules orderly distribute along the inner wall of CNTs with a radius of about  $4.8 \text{ \AA}$ . The analyses on RDF, the end-to-end distance and the torsion angle all suggest that CNT restricts the torsion of LA molecules and makes LA molecules have an orderly distribution in CNTs. The diffusion coefficient of LA molecules increases in CNTs.

The energy flux of LA molecules in CNTs is enhanced, which ultimately results in the thermal conductivity enhancement with 20 times compared with pure LA. The series behaviors are attributed to the nano-confined effect of CNTs and eventually result in the positive impact of heat and mass transfer of the system. Based on the experimental results, the MD method gives an interpretation of the phase change property of current systems from microcosmic perspective, and it could also be a guide for further experimental work.

**Acknowledgements** The work was supported by the National Nature Science Foundation of China (Grant 51206071), the Hunan Provincial Natural Science Foundation of China (Grant 13JJ6040) and the China Postdoctoral Science Foundation (Grant 2013M542125).

## References

1. Lv P, Liu C, Rao Z. Review on clay mineral-based form-stable phase change materials: preparation, characterization and applications. *Renew Sustain Energy Rev.* 2017;68(Part 1):707–26.
2. Khan Z, Khan Z, Ghafoor A. A review of performance enhancement of PCM based latent heat storage system within the context of materials, thermal stability and compatibility. *Energy Convers Manag.* 2016;115(Supplement C):132–58.
3. Wu S, Zhu D, Zhang X, Huang J. Preparation and melting/freezing characteristics of Cu/paraffin nanofluid as phase-change material (PCM). *Energy Fuels.* 2010;24(3):1894–8.
4. Yuan Y, Zhang N, Tao W, Cao X, He Y. Fatty acids as phase change materials: a review. *Renew Sustain Energy Rev.* 2014;29(Supplement C):482–98.
5. Wang Z, Sun J, Xie S, Ma G, Jia Y. Thermal properties and reliability of a lauric acid/nonanoic acid binary mixture as a phase-change material for thermal energy storage. *Energy Technol.* 2017;5(12):2309–16.
6. Cheng W-L, Li W-W, Nian Y-L, Xia W-D. Study of thermal conductive enhancement mechanism and selection criteria of carbon-additive for composite phase change materials. *Int J Heat*



- Mass Transf. 2018;116(Supplement C):507–11. <https://doi.org/10.1016/j.ijheatmasstransfer.2017.09.032>.
7. Li Y, Yan H, Wang Q, Wang H, Huang Y. Structure and thermal properties of decanoic acid/expanded graphite composite phase change materials. *J Therm Anal Calorim.* 2017;128(3):1313–26.
  8. Zhou Y, Sheng D, Liu X, Lin C, Ji F, Dong L, et al. Synthesis and properties of crosslinking halloysite nanotubes/polyurethane-based solid-solid phase change materials. *Sol Energy Mater Sol Cells.* 2018;174(Supplement C):84–93. <https://doi.org/10.1016/j.solmat.2017.08.031>.
  9. Genc M, Karagoz Genc Z. Microencapsulated myristic acid–fly ash with TiO<sub>2</sub> shell as a novel phase change material for building application. *J Therm Anal Calorim.* 2017;15:21–6. <https://doi.org/10.1007/s10973-017-6781-7>.
  10. Zeng J-L, Sun S-L, Zhou L, Chen Y-H, Shu L, Yu L-P, et al. Preparation, morphology and thermal properties of microencapsulated palmitic acid phase change material with polyaniline shells. *J Therm Anal Calorim.* 2017;129(3):1583–92.
  11. Fischer JE. Carbon nanotubes: structure and properties. 2006.
  12. Wu SY, Tong X, Nie CD, Peng DQ, Gong SG, Wang ZQ. The effects of various carbon nanofillers on the thermal properties of paraffin for energy storage applications. *J Therm Anal Calorim.* 2016;124(1):181–8.
  13. Fan L-W, Fang X, Wang X, Zeng Y, Xiao Y-Q, Yu Z-T, et al. Effects of various carbon nanofillers on the thermal conductivity and energy storage properties of paraffin-based nanocomposite phase change materials. *Appl Energy.* 2013;110:163–72.
  14. Temel UN, Kurtulus S, Parlak M, Yapici K. Size-dependent thermal properties of multi-walled carbon nanotubes embedded in phase change materials. *J Therm Anal Calorim* 1–11.
  15. Miners SA, Rance GA, Khlobystov AN. Chemical reactions confined within carbon nanotubes. *Chem Soc Rev.* 2016;45(17):4727–46.
  16. Mattia D, Gogotsi Y. Review: static and dynamic behavior of liquids inside carbon nanotubes. *Microfluid Nanofluid.* 2008;5(3):289–305.
  17. Gradys A. Geometrical effects during crystallization under confinement in electrospun core-shell fibers. DSC study of crystallization kinetics. *Polymer.* 2017;108(Supplement C):383–94.
  18. Sinha-Ray S, Sinha-Ray S, Sriram H, Yarin AL. Flow of suspensions of carbon nanotubes carrying phase change materials through microchannels and heat transfer enhancement. *Lab Chip.* 2014;14(3):494–508.
  19. Sinha-Ray S, Sahu RP, Yarin AL. Nano-encapsulated smart tunable phase change materials. *Soft Matter.* 2011;7(19):8823–7.
  20. Aoun B, Russo D. Nano-confinement of biomolecules: hydrophilic confinement promotes structural order and enhances mobility of water molecules. *Nano Res.* 2016;9(2):273–81.
  21. Thomas JA, Iutzi RM, McGaughey AJHM. Thermal conductivity and phonon transport in empty and water-filled carbon nanotubes. *Phys Rev B.* 2010;81:045413.
  22. Liang W, Wu Y, Sun H, Zhu Z, Chen P, Yang B, et al. Halloysite clay nanotubes based phase change material composites with excellent thermal stability for energy saving and storage. *RSC Adv.* 2016;6(24):19669–75.
  23. Zhang H, Rindt CCM, Smeulders DMJ, Nedeia SV. Nanoscale heat transfer in carbon nanotubes—sugar alcohol composite as heat storage materials. *J Phys Chem C.* 2016;120:21915–24.
  24. Jeong N, Park YC, Yoo JH. Preparation of highly pure and crystalline carbon nanotubes and their infiltration by paraffin wax. *Carbon.* 2013;63:240–52.
  25. Pascal TA, Goddard WA, Jung Y. Entropy and the driving force for the filling of carbon nanotubes with water. *Proc Natl Acad Sci.* 2011;108(29):11794–8.
  26. Liu X, Lin C, Rao Z. Diffusion and thermal conductivity of the mixture of paraffin and polystyrene for thermal energy storage: a molecular dynamics study. *J Energy Inst.* 2017;90(4):534–43.
  27. Srinivasan S, Diallo MS, Saha SK, Abass OA, Sharma A, Balasubramanian G. Effect of temperature and graphite particle fillers on thermal conductivity and viscosity of phase change material n-eicosane. *Int J Heat Mass Transf.* 2017;114(Supplement C):318–23. <https://doi.org/10.1016/j.ijheatmasstransfer.2017.06.081>.
  28. Rao Z, Wang S, Peng F. Molecular dynamics simulations of nano-encapsulated and nanoparticle-enhanced thermal energy storage phase change materials. *Int J Heat Mass Transf.* 2013;66:575–84.
  29. Babaei H, Keblinski P, Khodadadi JM. Thermal conductivity enhancement of paraffins by increasing the alignment of molecules through adding CNT/graphene. *Int J Heat Mass Transf.* 2013;58(1–2):209–16.
  30. Changda Nie XT, Shuying Wu. Shuguang Gong and Deqi Peng. Paraffin confined in carbon nanotubes as nano-encapsulated phase change materials: experimental and molecular dynamics studies. *RSC Adv.* 2015;5:92812–7.
  31. Tong X, Wu S, Peng D, Gong S. Distribution and thermophysical properties of n-heptacosane molecules confined in carbon nanotube. *Phase Transit.* 2016;89(3):598–607.
  32. Iwahashi M, Kasahara Y, Minami H, Matsuzawa H, Suzuki M, Ozaki Y. Molecular behaviors of n-fatty acids in liquid state. *J Oleo Sci.* 2002;51(3):157–64.
  33. Müller-Plathe F. A simple nonequilibrium molecular dynamics method for calculating the thermal conductivity. *J Chem Phys.* 1997;106(14):6082–5.
  34. Lu W, Punyamurtula VK, Qiao Y. An energy absorption system based on carbon nanotubes and non-aqueous liquid. *Int J Mater Res.* 2011;102(5):587–90.
  35. Tao W, He Y, Wang Q, Qu Z, Song F. A unified analysis on enhancing single phase convective heat transfer with field synergy principle. *Int J Heat Mass Transf.* 2002;45(24):4871–9.
  36. Zhou G, Zhao T, Wan J, Liu C, Liu W, Wang R. Predict the glass transition temperature and plasticization of  $\beta$ -cyclodextrin/water binary system by molecular dynamics simulation. *Carbohydr Res.* 2015;401:89–95.
  37. Wei S, Zhong C, Su-Yi H. Molecular dynamics simulation of liquid water under the influence of an external electric field. *Mol Simul.* 2005;31(8):555–9.
  38. Yang Y, Zhang Q, Pan Y, Long L, Zheng L. Magnetocaloric effect and thermal conductivity of Gd(OH)<sub>3</sub> and Gd<sub>2</sub>O(OH)<sub>4</sub>(-H<sub>2</sub>O)<sub>2</sub>. *Chem Commun.* 2015;51(34):7317–20.
  39. Harish S, Orejon D, Takata Y, Kohno M. Thermal conductivity enhancement of lauric acid phase change nanocomposite in solid and liquid state with single-walled carbon nanohorn inclusions. *Thermochim Acta.* 2015;600(Supplement C):1–6.
  40. Marconnet AM, Panzer MA, Goodson KE. Thermal conduction phenomena in carbon nanotubes and related nanostructured materials. *Rev Mod Phys.* 2013;85(3):1295.
  41. Zhang N, Yuan Y, Cao X, Du Y, Zhang Z, Gui Y. Latent heat thermal energy storage systems with solid–liquid phase change materials: a review. *Adv Eng Mater.* 2018; 1700753.
  42. Yamada Y, Askounis A, Ikuta T, Takahashi K, Takata Y, Sefiane K. Thermal conductivity of liquid/carbon nanotube core-shell nanocomposites. *J Appl Phys.* 2017;121(1):015104.
  43. Cui L, Feng Y, Zhang X. Enhancement of heat conduction in carbon nanotubes filled with fullerene molecules. *PCCP.* 2015;17(41):27520–6.